Available online at www.sciencedirect.com
SCIENCE DIRECT®
Journal of Sound and Vibration 291 (2006) 349–368
JOURNAL OF SOUND AND VIBRATION
www.elsevier.com/locate/jsvi

Time series-based damage detection and localization algorithm with application to the ASCE benchmark structure

K. Krishnan Nair[a], Anne S. Kiremidjian[b,*], Kincho H. Law[b]

[a]*John A. Blume Earthquake Engineering Center, Department of Civil and Environmental Engineering, Stanford University, Stanford, CA 94305, USA*
[b]*Department of Civil and Environmental Engineering, Stanford University, Stanford, CA 94305, USA*

Received 13 January 2005; received in revised form 12 May 2005; accepted 14 June 2005
Available online 12 September 2005

Abstract

In this paper, a time series algorithm is presented for damage identification and localization. The vibration signals obtained from sensors are modeled as autoregressive moving average (ARMA) time series. A new damage-sensitive feature, DSF, is defined as a function of the first three auto regressive (AR) components. It is found that the mean values of the DSF for the damaged and undamaged signals are different. Thus, a hypothesis test involving the *t*-test is used to obtain a damage decision. Two damage localization indices LI_1 and LI_2, are introduced based on the AR coefficients. At the sensor locations where damage is introduced, the values of LI_1 and LI_2 appear to increase from their values obtained at the undamaged baseline state. The damage detection and localization algorithms are valid for stationary signals obtained from linear systems. To test the efficacy of the damage detection and localization methodologies, the algorithm has been tested on the analytical and experimental results of the ASCE benchmark structure. In contrast to prior pattern classification and statistical signal processing algorithms that have been able to identify primarily severe damage and have not been able to localize the damage effectively, the proposed algorithm is able to identify and localize minor to severe damage as defined for the benchmark structure.

*Corresponding author. Tel.: +1 650 723 4164; fax: +1 650 723 7514.
E-mail addresses: kknair@stanford.edu (K.K. Nair), ask@stanford.edu (A.S. Kiremidjian), law@stanford.edu (K.H. Law).

0022-460X/$ - see front matter © 2005 Elsevier Ltd. All rights reserved.
doi:10.1016/j.jsv.2005.06.016

1. Introduction and motivation

Structural health monitoring has become of great significance in the civil engineering community in the last few years [1]. There is a need to continuously monitor the level of performance and safety of structures, while subjected to everyday loads as well as earthquakes, hurricanes and other extreme events, due to increased safety requirements and financial implications. Recent research has demonstrated that wireless sensing networks can be successfully used for structural health monitoring [2,3]. Low cost microeletromechanical sensors (MEMS) and wireless solutions have been fabricated for structural measurement and this allows for a dense network of sensors to be deployed in structures.

Most currently available damage detection methods are global in nature, i.e., the dynamic properties (natural frequencies and mode shapes) are obtained for the entire structure from the input–output data using a global structural analysis [4]. However, global damage measures are not sensitive to minor damage and local damage. Furthermore, such methods involve finite element modeling and system identification methods, which can be computationally expensive.

In the past few years, methods have been developed that utilize statistical signal processing techniques to identify damage [5,6]. Such methods rely on the signatures obtained from the recorded vibration, strain or other data to extract features that change with the onset of damage. These features can then be classified in a pattern classification framework. A pattern classification algorithm involves the following steps: (i) the evaluation of a structure's operational environment, (ii) the acquisition of structural response measurements and data processing, (iii) the extraction of features that are sensitive to damage, and (iv) the development of statistical models for feature discrimination. These methods avoid the complexity of global system identification techniques and are particularly suitable for ongoing monitoring purposes. Furthermore, they may serve as a technique for data reduction that will minimize the amount of data needed to be transmitted by the radio of the wireless monitoring node.

Structural health monitoring involves the following steps, (a) diagnosis, which includes damage identification, damage localization and damage level assessment and (b) prognosis, which includes structure's residual capacity estimation and residual life forecasting [7]. In this paper, damage identification and localization are investigated in a pattern classification framework. A new damage-sensitive feature (DSF) based on the autoregressive (AR) coefficients is presented. It is found that there is a difference in the mean values of the DSF of the signals obtained from the *damaged* and *undamaged* cases. The relationship between the AR coefficients used in the DSF and the physical parameters of the system are investigated in Appendix A. It is shown that the AR coefficients are related to poles of the mechanical system that is investigated and as expected, changes in stiffness are manifested as changes in the AR coefficients. From t-tests, it is seen that the difference in the means of the DSFs of the damaged and undamaged signals is statistically significant. For localizing the damage, two localization indices, defined in the AR coefficient space, are proposed. The algorithm has been tested on several data sets from the ASCE benchmark structure [8]. Both the numerical simulation data [9] and the experimental data [10] have been used.

The paper first summarizes the autoregressive moving average (ARMA) modeling aspects of the vibration signals. The variation of DSF for each damage pattern is discussed next. Hypothesis testing using the t-test and localization using LI are explained and then the results of the

applications of the algorithm on the ASCE benchmark structure are presented. The sensitivity of the eigenvalues and eigenvectors are summarized in Appendix A.

2. Description of the damage algorithm

Structural damage affects the dynamic properties of a structure, resulting in a change in the statistical characteristics of the measured acceleration time histories. Thus, damage detection can be performed using time series analysis of vibration signals measured from a structure before and after damage. In this study, we use the ARMA time series to model the vibration data obtained from the sensor. The analysis is limited to linear vibration data (before and after the event) and the assumption is made that after damage has taken place, the structure is still behaving linearly under normal every day loads even though its properties may have changed. Thus, the present study is limited to linear stationary signals.

2.1. Modeling of the vibration signals

A typical vibration signal from Sensor 1 is shown in Fig. 1. Before fitting the ARMA models to the sensor data, it is important to perform standardization (or normalization) in order to compare acceleration time histories (at a sensor location) that may have occurred due to different loading conditions (i.e., different magnitudes and directions of loads) and/or different environmental conditions. After normalization the features extracted from the signals from undamaged cases would have similar statistical characteristics and can be compared.

Let $x_i(t)$ be the acceleration data from sensor i. This sensor data is then partitioned into different streams $x_{ij}(t)$, where i denotes the sensor number and j denotes the jth stream of data

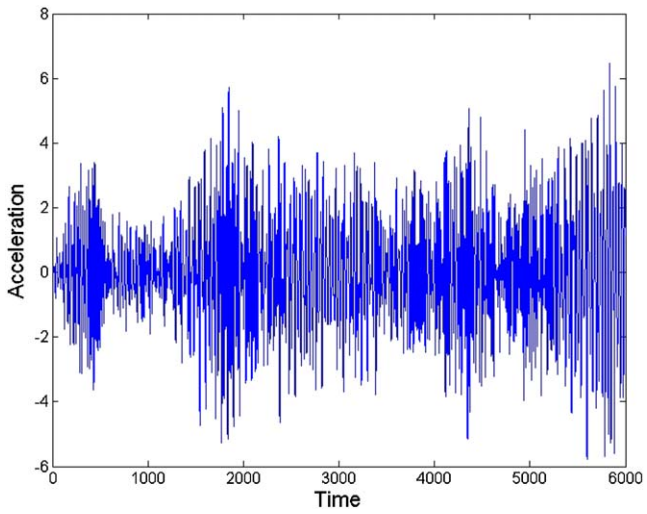

Fig. 1. A typical raw acceleration time history from an undamaged case serving as the reference signal for subsequent damage detection (Sensor 2).

from the sensor i. Then, the normalized signal $\tilde{x}_{ij}(t)$ is obtained as follows:

$$\tilde{x}_{ij}(t) = \frac{x_{ij}(t) - \mu_{ij}}{\sigma_{ij}}, \tag{1}$$

where μ_{ij} and σ_{ij} are the mean and standard deviation of the jth stream of sensor I, respectively. For notational convenience, $x_{ij}(t)$ will be used instead of $\tilde{x}_{ij}(t)$. The next step is to check for trends and stationarity in the data [11]. This can be done by observing the autocorrelation function (ACF). Fig. 2 shows that the ACF of the normalized data has a cyclical trend that will need to be removed. For detrending the data, three methods are used, (i) harmonic regression, (ii) simple average window and (iii) moving average window [11]. It is found that harmonic regression could not remove the trends and thus a combination of the simple average window and the moving average window is used. The window sizes are chosen so that the residuals obtained from this process are stationary. A review of the autocorrelation plot or the Ljung–Box statistic provides further test that this condition is preserved. A more detailed explanation is provided in subsequent sections.

Once the initial data pre-processing is complete, the optimal ARMA model order and its coefficients are estimated [11]. The ARMA model is given by

$$x_{ij}(t) = \sum_{k=1}^{p} \alpha_k x_{ij}(t-k) + \sum_{k=1}^{q} \beta_k \varepsilon_{ij}(t-k) + \varepsilon_{ij}(t), \tag{2}$$

where $x_{ij}(t)$ is the normalized acceleration signal, α_k and β_k are the kth AR and MA coefficient, respectively; p and q are the model orders of the AR and MA processes, respectively, and $\varepsilon_{ij}(t)$ is the residual term.

The Burg algorithm (also known as the maximum entropy method) is used for estimating the coefficients of the ARMA process [11]. The optimal model order is obtained using the Akaike

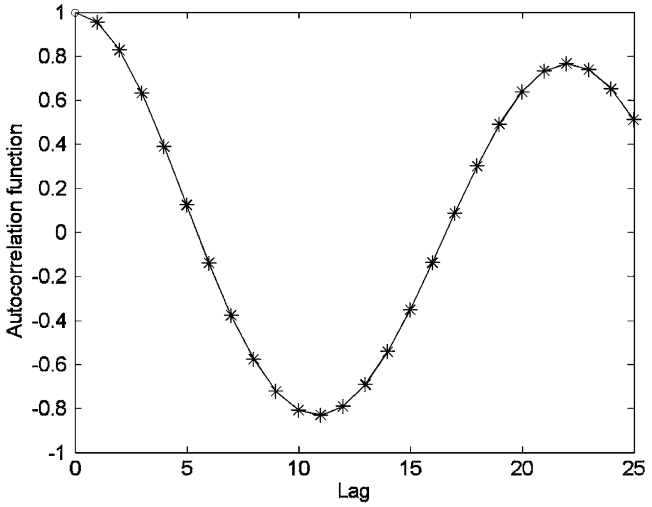

Fig. 2. Autocorrelation function of the normalized data.

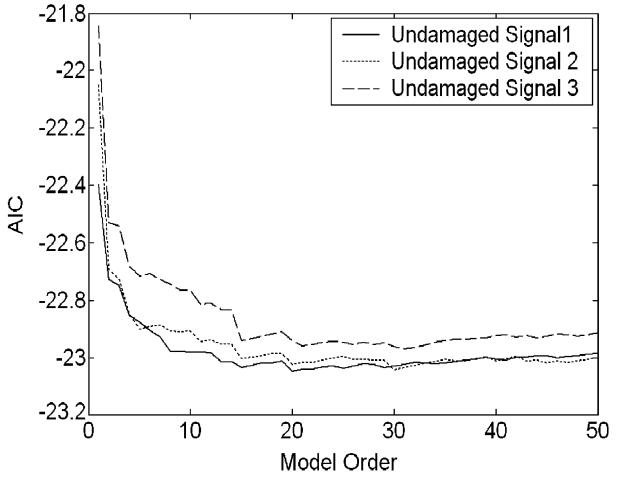

Fig. 3. Variation of AIC with model order.

information criteria (AIC) [11]. The AIC consists of two terms, one of which is a log-likelihood function and the other term, which penalizes the number of terms in the ARMA model. Fig. 3 shows the variation of the AIC values with the AR model order. It is seen that an AR model order of 5–8 and MA model order of 2–4 is appropriate for the analysis. Also, a cross-validation analysis is carried out to check the accuracy of the results. For a particular data stream, the data set is split in two, one is used for the analysis and the other is used for forecasting. In the analysis part, the coefficients of the ARMA model are ascertained. Using these coefficients, the values of the acceleration data are predicted. The error between the predicted values and actual values are obtained to be a minimum using the above model orders.

In order to obtain the AR and MA coefficients the Burg Algorithm is applied. Then the residuals obtained are tested to determine if they are normal and independent and identically distributed (i.i.d.). Fig. 4(a) shows the normal probability plot of the residuals. The straight line variation indicates a normal distribution of the data, which is violated at the tails. Fig. 4(b) shows the variation of the residuals with time. It is seen that there is no trend, therefore, indicating homoskedasticity. Fig. 4(c) shows the ACF of the residuals, from which it is observed that the values of the ACF at lags greater than one are not statistically significant. The Ljung–Box statistic is also used to test the i.i.d. assumption of the ARMA residuals. The Ljung–Box statistic is defined as follows:

$$Q_{\mathrm{LB}} = n(n+2)\sum_{j=1}^{h}\frac{\rho^2(j)}{n-j}, \tag{3}$$

where n is the sample size, $\rho(j)$ is the autocorrelation function at lag j, and h is the number of lags being tested. The null hypothesis of randomness is rejected if $Q_{\mathrm{LB}} > \chi^2_{1-\alpha,h}$, where α is the level of significance of the hypothesis test and $\chi^2_{1-\alpha,h}$ is the $(1-\alpha)$th percentile of the χ^2 distribution with h degrees of freedom. For this particular data set, the null hypothesis is accepted. Thus, the assumptions made on the residuals are satisfied.

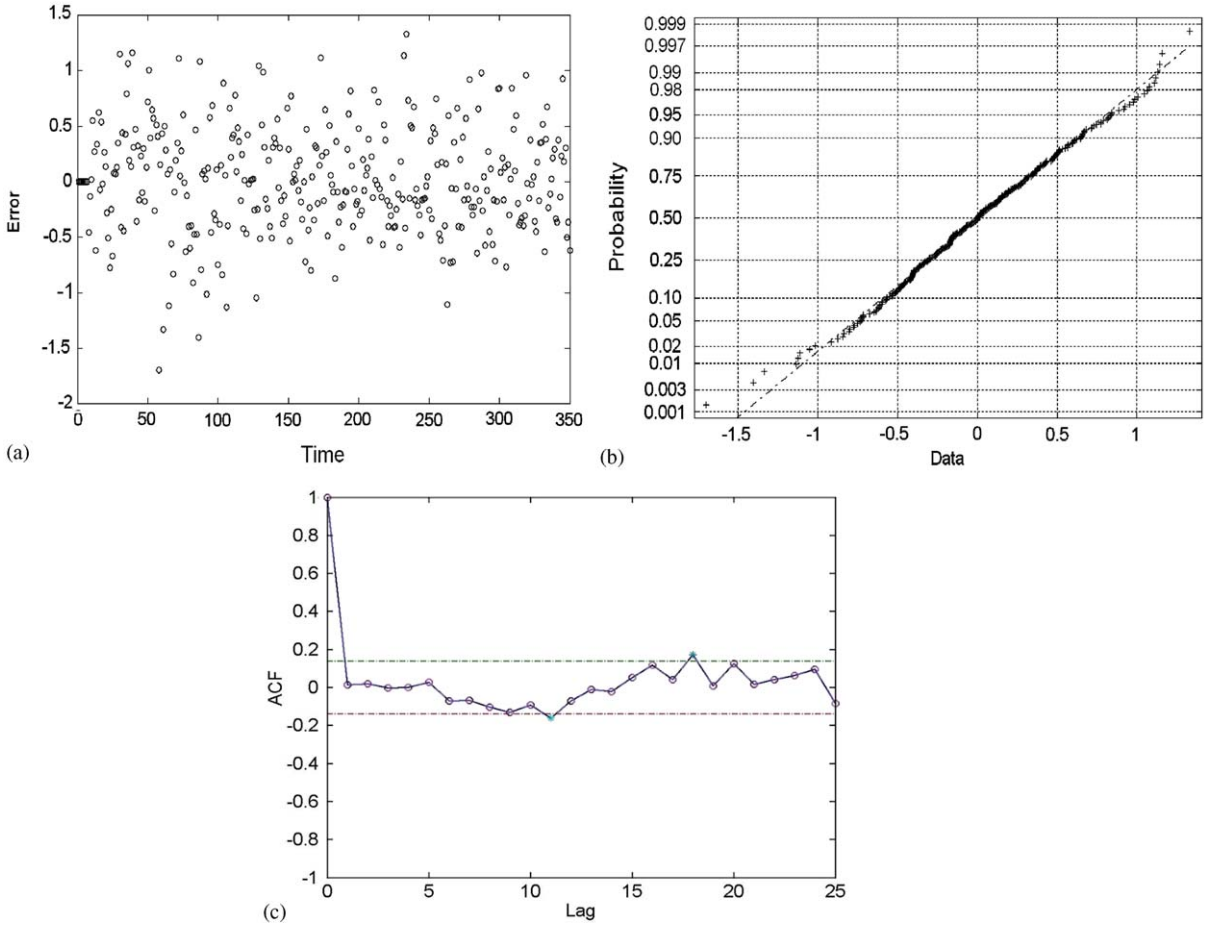

Fig. 4. Verification of the i.i.d. characteristics and normality of residuals. (a) Variation of residuals with time. (b) Normal probability plot of the residuals. (c) Variation of the autocorrelation function of the residuals with lag.

2.2. Definition and development of the DSF

In this section, the ARMA time series model is used to develop features that discriminate between damage and non-damaged state of a structure. Several DSF were considered. Of those various DSFs considered, those depending on the first three AR coefficients appeared to be most promising because these coefficients are statistically the most significant among all the coefficients of the model. After testing several different combinations with the first three coefficients, it was found that the first AR coefficient normalized by the square root of the sum of the squares of the first three AR coefficients provides the most robust DSF. Thus the proposed DSF is defined as follows:

$$\mathrm{DSF} = \frac{\alpha_1}{\sqrt{\alpha_1^2 + \alpha_2^2 + \alpha_3^2}}, \tag{4}$$

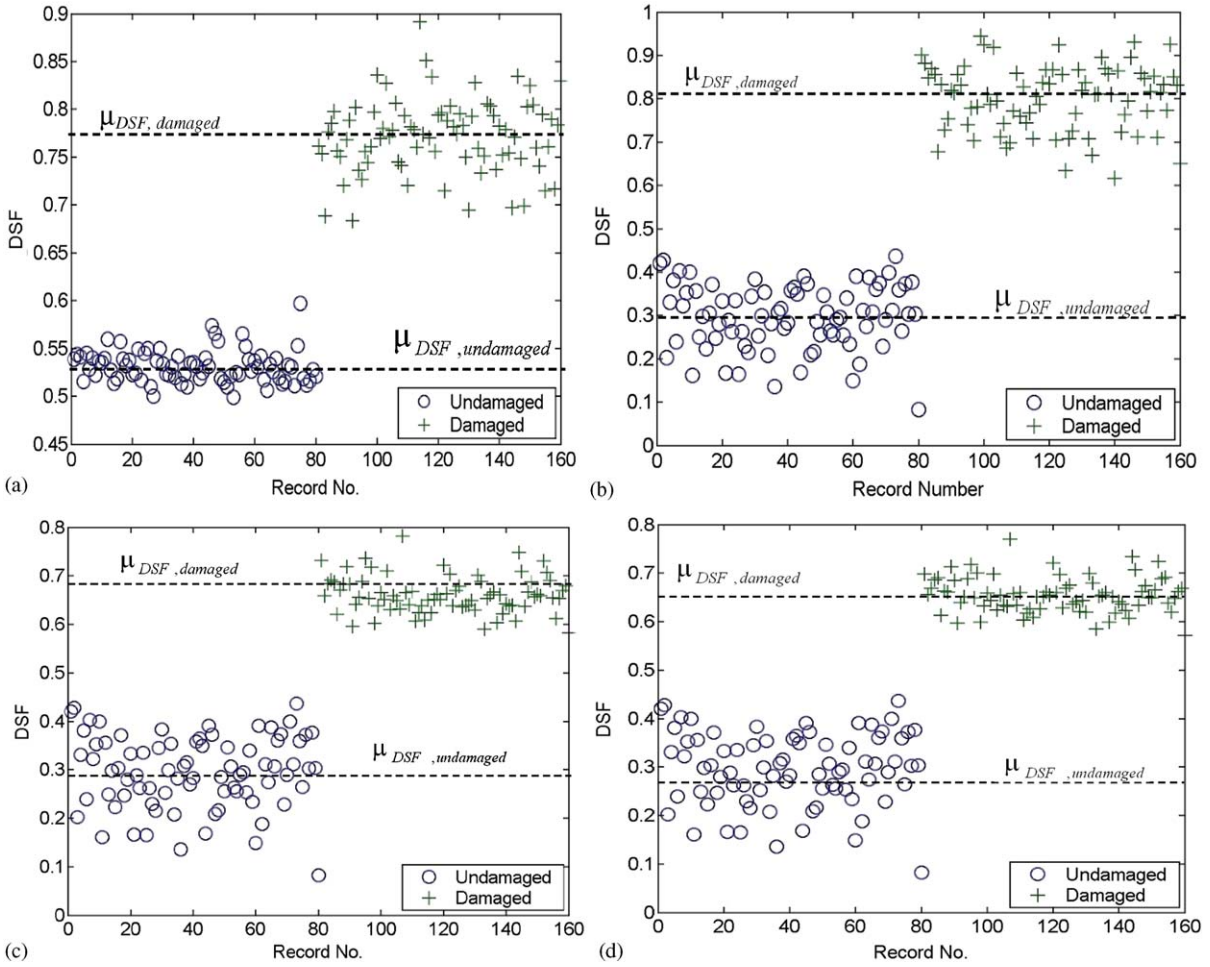

Fig. 5. Variation of DSF with record number for different damage patterns. (a) Damage pattern 1. (b) Damage pattern 2. (c) Damage pattern 3. (d) Damage pattern 4.

where α_1, α_2 and α_3 are the first three AR coefficients. Variations of the DSF with the record number for different damage patterns is illustrated in Figs. 5(a)–(d). From these figures it can be seen that for all damage patterns there is a significant difference in the mean levels of the DSFs of the damaged and the undamaged states. Thus, to test statistical difference between the means of two groups of data, the standard t-test is used [12].

A heuristic understanding of the above DSF is given here. The AR coefficients generally contain information about the modal natural frequencies and the damping ratios [13,14]. The ARMA model in the context of the linear input vibration (assuming to be white noise) may then be treated as an autoregressive model with exogenous input (ARX) time series. This model can be examined in the complex z domain by applying the time-shifting property of the z-transform [15].

The z-transform of a function $f(t)$, denoted by $F(z)$, is defined as follows [15]:

$$F(z) = \sum_{k=-\infty}^{\infty} f(k) z^{-k}. \tag{5}$$

Consider a signal shifted by a time units, $f(t-a)$. The z-transform of $f(t-a)$ is given as follows:

$$Z[f(t-a)] = z^{-a} F(z). \tag{6}$$

This is known as the time shifting property of the z-transform.

Applying the z-transform to both sides of Eq. (2) and ignoring the effect of the error term, we obtain

$$X_{ij}(z) = \sum_{k=1}^{p} \alpha_k z^{-k} X_{ij}(z) + \sum_{k=1}^{q} \beta_k z^{-k} \Xi_{ij}(z), \tag{7}$$

where $X_{ij}(z)$ and $\Xi_{ij}(z)$ are the z-transforms of the $x_{ij}(t)$ and $\varepsilon_{ij}(t)$, respectively. Then, the transfer function $H(z)$ is derived as

$$H(z) = \frac{X_{ij}(z)}{\Xi_{ij}(z)} = \frac{\beta_1 z^{-1} + \beta_2 z^{-2} + \cdots + \beta_q z^{-q}}{1 - \alpha_1 z^{-1} - \alpha_2 z^{-2} - \cdots - \alpha_p z^{-p}}. \tag{8}$$

The denominator of the transfer function $[H(z)]$ is a polynomial equation of order p known as the characteristic equation. The roots of the characteristic equation, known as the poles of the system, are expressed as follows:

$$\left[z^p - \alpha_1 z^{p-1} - \alpha_2 z^{p-2} - \cdots - \alpha_p\right] = 0. \tag{9}$$

The poles, z_{pole}, of the characteristic equation are a good indicator of the modal natural frequencies and the damping ratios given by [13]

$$z_{\text{pole}} = \mathrm{e}^{\left[-\xi\omega_n \Delta t \pm \mathrm{j}\sqrt{1-\xi^2}\omega_n \Delta t\right]}, \tag{10}$$

where ξ and ω are the damping ratio and natural frequency of the particular mode and Δt is the sampling time of the signal. This may also be rewritten as $z_{\text{pole}} = r\mathrm{e}^{\mathrm{j}\phi}$, where the amplitude r and phase angle ϕ are expressed as

$$r = \mathrm{e}^{-\xi\omega_n \Delta t}, \tag{11a}$$

$$\phi = \sqrt{1-\xi^2}\omega_n \Delta t. \tag{11b}$$

Using simple theory of polynomial roots, it can be shown that

$$\sum_i z_{\text{pole},i} = \alpha_1, \tag{12a}$$

$$\sum_{i,j} z_{\text{pole},i} z_{\text{pole},j} = -\alpha_2, \tag{12b}$$

$$\sum_{i,j,k} z_{\text{pole},i} z_{\text{pole},j} z_{\text{pole},k} = \alpha_3. \tag{12c}$$

Without loss of generality, p is assumed to be even and all the poles to be imaginary. Thus, Eq. (11a) can be rewritten as follows:

$$\alpha_1 = \sum_{i=1}^{p} z_{\text{pole},i} = \sum_{i=1}^{p/2} 2r_i \cos \phi_i. \tag{13}$$

Differentiating with respect to a parameter θ_i, say an element of the stiffness matrix, we obtain

$$\frac{\partial \alpha_1}{\partial \theta_i} = \frac{\partial \alpha_1}{\partial k_i}\frac{\partial k_i}{\partial \theta_i}, \tag{14}$$

where k_i is the ith modal stiffness. Differentiating with respect to k_i and assuming that the damping ratio is a constant in each mode, we get the following:

$$\begin{aligned}\frac{\partial \alpha_1}{\partial k_i} &= 2\frac{\partial r_i}{\partial k_i}\cos \phi_i + 2r_i(-\sin \phi_i)\frac{\partial \phi_i}{\partial k_i} \\ &= -\left(\frac{r_i \Delta t}{\sqrt{m_i k_i}}\right)\left[\xi_i \cos \phi_i + \sqrt{1-\xi_i^2}\sin \phi_i\right],\end{aligned} \tag{15}$$

where $\omega_{n,i}$ is the ith natural frequency, $r_i = \mathrm{e}^{-\xi_i \omega_{n,i}\Delta t}$ and $\phi_i = \sqrt{1-\xi_i^2}\,\omega_{n,i}\Delta t$. Taking the absolute value of the sensitivity $\partial\alpha_1/\partial k_i$ and since the sampling interval is generally small, we obtain

$$\left|\frac{\partial \alpha_1}{\partial k_i}\right| \approx \frac{\Delta t}{\sqrt{m_i k_i}}. \tag{16}$$

It is shown in Appendix A that $|\partial k_i/\partial \theta_i| \leqslant 1$ and thus we can conclude that $|\partial \alpha_1/\partial \theta_i| \leqslant \Delta t/\sqrt{m_i k_i}$.

Similar equations can be derived for $\partial\alpha_2/\partial\theta_i$ and $\partial\alpha_3/\partial\theta_i$. Thus, it can be concluded that as the stiffness decreases due to damage, the response of the structure will change resulting in changes of the AR coefficients. Consequently, the DSF based on the AR coefficients can capture this change in measurements from an undamaged to damaged structural state.

2.3. Damage localization indices

Fig. 6 shows the damaged and undamaged clouds in the AR coefficient space where two damage localization indices are defined as follows:

$$\text{LI}_1 = \frac{d_{\text{mean}}}{d_{\text{undam cloud}}}, \tag{17a}$$

$$\text{LI}_2 = \frac{d_{\text{dam cloud}}}{d_{\text{undam cloud}}}, \tag{17b}$$

where d_{mean} is the distance between the centers of the damaged and undamaged clouds, $d_{\text{dam cloud}}$ is the distance from the origin to the center of the damaged cloud and $d_{\text{undam cloud}}$ is the distance from the origin to the undamaged cloud.

The efficacy of these indices, DSF and LI, will be tested on the ASCE benchmark structure [9] and this is presented in a later section.

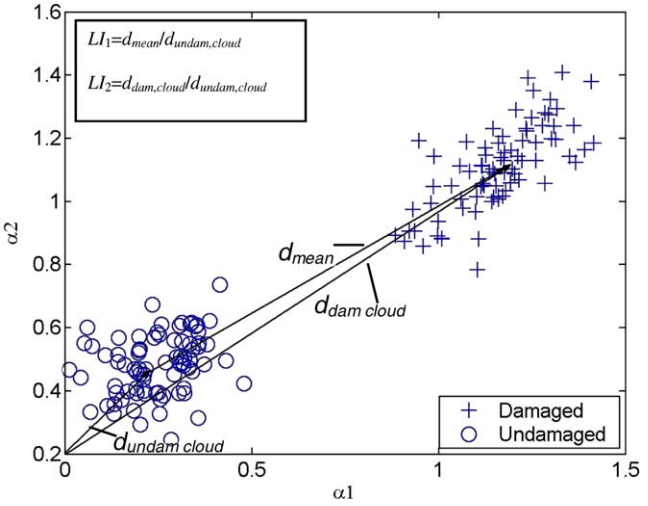

Fig. 6. Illustration of the localization index LI.

2.4. Damage-detection algorithm synthesis

The damage-detection algorithm is summarized in the following steps:

- Populate a database with signals from the undamaged structure at each sensor location $x_{ij}(t)$.
- Standardize signal to remove all trends and environmental conditions to obtain $\tilde{x}_{ij}(t)$.
- Obtain signal from $z_{ij}(t)$ from the ith sensor of the structure (whose condition we are to ascertain) and standardize this signal as shown above.
- Fit an ARMA model to all data streams including $\tilde{z}_{ij}(t)$.
- Define and compute the mean values of DSF for the pre- and post-event signals.
- Determine the statistical significance in the differences of mean values of the pre- and post-event data using the t-test to report damage decision.
- Calculate the LI for each sensor.

The advantage of the damage-detection algorithm presented in this section is that it depends on signals obtained at a specified location on of a structure. With current smart sensing capabilities that provide computational power at the sensor location, the algorithm can be embedded and executed at the data collection site. Because of its simplicity, the algorithm also can be executed rapidly and efficiently providing critical information in a timely manner.

3. Application results

In order to test the validity of the algorithm, results from the numerical simulation and laboratory experiments of the ASCE benchmark structure are used. The structure is a four story, two-bay × two-bay steel-braced frame, illustrated in Fig. 7 [9]. The location of the accelerometers

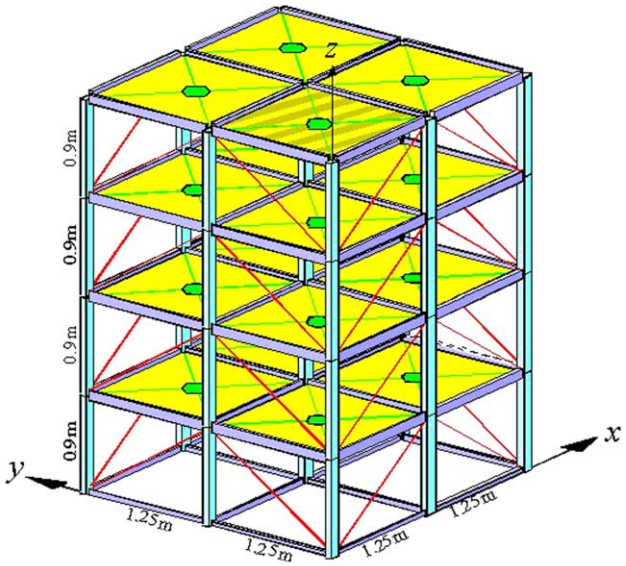

Fig. 7. Diagram of the ASCE benchmark structure [9].

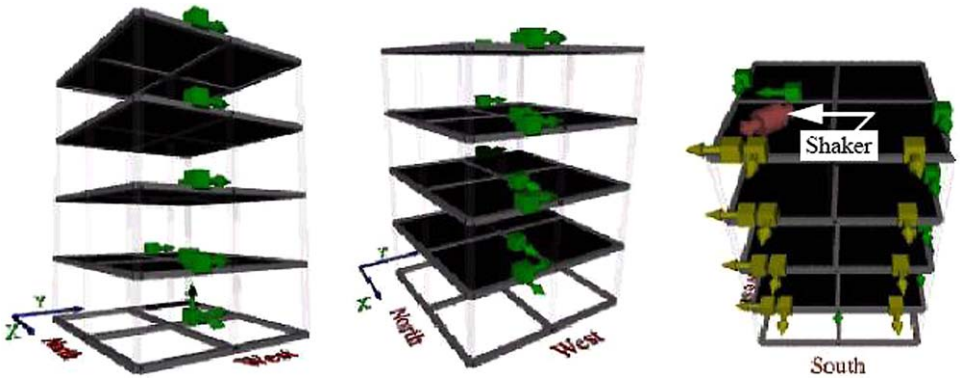

Fig. 8. Placement of sensors and location of shaker in the experimental ASCE benchmark structure [10].

and the loading on the structure are also identified in Fig. 8 [10]. It can be seen that the structure is subjected to shaking at the top story. Damage is simulated by removing braces in various combinations, resulting in a loss of stiffness. Damage patterns include

- Damage pattern 1: Removal of all braces on the first floor.
- Damage pattern 2: Removal of all braces on the first and third floors.
- Damage pattern 3: Removal of one brace on the first floor.
- Damage pattern 4: Removal of one braces on the first and third floors.

Damage patterns 1 and 2 are major damage patterns, whereas damage patterns 3 and 4 are minor damage patterns.

In this study, results from the numerical simulation [9] and the experimental study [10] are included. In the numerical study, two finite element models were used to generate the simulated response data: a 12-degree-of-freedom (dof) shear-building model that constrains all motion except two horizontal translations and one rotation per floor and the second is a 120-dof model that requires that floor nodes have the same horizontal translation and in-plane rotation. The columns and floor beams are modeled as Euler–Bernoulli beams and the braces have no flexural stiffness.

In the experimental benchmark, the force input to the structure was provided by a shaker placed on the top floor of the structure along the diagonal in the center of the southwest bay (see Fig. 8). Data from the DasyLab Acquisition system is used [10]. The sampling frequency of the data set is 250 Hz.Also, it should be noted that channel 6 of the DasyLab system was not operating correctly during the test and thus is not used in this study. We consider only damage patterns C and D, defined as follows:

- Damage pattern C: Removal of a brace from the north face, west bay on the first floor (similar to damage pattern 3).
- Damage pattern D: Removal of a brace from the north face, west bay on the first floor the first and third floors (similar to damage pattern 4).

3.1. Damage detection

Fig. 5 shows the results from the application of the proposed damage algorithm to the numerically simulated data sets of the ASCE benchmark structure. From Figs. 5(a)–(d), it can be observed that there is a significant difference between the mean values of the DSFs obtained from the damaged and undamaged cases. If $\mu_{\mathrm{DSF,\,damaged}}$ and $\mu_{\mathrm{DSF,\,undamaged}}$ are defined as the mean values of the DSFs obtained from the damaged and undamaged case, respectively, then a hypothesis test may be set up as follows to determine if their differences are significant:

$$\begin{aligned} &\mathrm{H}_0 : \mu_{\mathrm{DSF,\,undamaged}} = \mu_{\mathrm{DSF,\,damaged}}, \\ &\mathrm{H}_1 : \mu_{\mathrm{DSF,\,undamaged}} \neq \mu_{\mathrm{DSF,\,damaged}}, \end{aligned} \tag{18}$$

where H_0 and H_1 are the null and alternate hypothesis, respectively. H_0 represents the undamaged condition and H_1 represents the damaged condition. The significance level of the test is set at 0.05.

Tables 1–4 show the results of the damage decision results for damage patterns 1–4 for the numerical simulation study. It is observed that for all of the cases the damage decision for all of the sensors give H_1, which indicates damage in the structure. The p-value is the probability that the DSF does not predict damage, given in fact that there is damage in the structure. Since the p-values are all significantly much less than the significance level of 0.05, the null hypothesis H_0 is rejected and the alternate hypothesis H_1 is accepted.

Tables 5 and 6 show the results of the damage decision for damage patterns C and D in the experimental benchmark study. Although most of the sensors do show H_1, Sensors 11 and 3 give

Table 1
Results of damage decision for damage pattern 1 (simulated)

Sensor No.	Damage decision	p-value
1	H_1	≈ 0.0
2	H_1	≈ 0.0
3	H_1	≈ 0.0
4	H_1	≈ 0.0
5	H_1	≈ 0.0
6	H_1	≈ 0.0
7	H_1	≈ 0.0
8	H_1	≈ 0.0
9	H_1	6.260×10^{-6}
10	H_1	≈ 0.0
11	H_1	≈ 0.0
12	H_1	≈ 0.0
13	H_1	≈ 0.0
14	H_1	≈ 0.0
15	H_1	1.200×10^{-6}
16	H_1	1.875×10^{-5}

Table 2
Results of damage decision for damage pattern 2 (simulated)

Sensor No.	Damage decision	p-value
1	H_1	≈ 0.0
2	H_1	≈ 0.0
3	H_1	≈ 0.0
4	H_1	≈ 0.0
5	H_1	≈ 0.0
6	H_1	≈ 0.0
7	H_1	≈ 0.0
8	H_1	≈ 0.0
9	H_1	≈ 0.0
10	H_1	≈ 0.0
11	H_1	≈ 0.0
12	H_1	≈ 0.0
13	H_1	2.204×10^{-6}
14	H_1	≈ 0.0
15	H_1	8.265×10^{-6}
16	H_1	≈ 0.0

the decision H_0 for cases C and D, respectively. Since H_0 indicates no damage, it gives a Type II error. However, it should be noted that the p-values for both these cases are very close to 0.05 and thus more investigation is required.

Table 3
Results of damage decision for damage pattern 3 (simulated)

Sensor No.	Damage decision	*p*-value
1	H_1	≈ 0.0
2	H_1	≈ 0.0
3	H_1	≈ 0.0
4	H_1	≈ 0.0
5	H_1	3.096×10^{-6}
6	H_1	9.385×10^{-6}
7	H_1	≈ 0.0
8	H_1	≈ 0.0
9	H_1	4.654×10^{-6}
10	H_1	≈ 0.0
11	H_1	≈ 0.0
12	H_1	≈ 0.0
13	H_1	≈ 0.0
14	H_1	6.304×10^{-6}
15	H_1	3.105×10^{-6}
16	H_1	0.001056

Table 4
Results of damage decision for damage pattern 4 (simulated)

Sensor No.	Damage decision	*p*-value
1	H_1	≈ 0.0
2	H_1	≈ 0.0
3	H_1	≈ 0.0
4	H_1	≈ 0.0
5	H_1	≈ 0.0
6	H_1	7.945×10^{-6}
7	H_1	≈ 0.0
8	H_1	≈ 0.0
9	H_1	≈ 0.0
10	H_1	≈ 0.0
11	H_1	≈ 0.0
12	H_1	≈ 0.0
13	H_1	≈ 0.0
14	H_1	1.345×10^{-6}
15	H_1	7.742×10^{-6}
16	H_1	0.009104

3.2. Damage localization

The results of the damage localization indices LI_1 and LI_2 are illustrated in Tables 7–10. For damage pattern 1 (Table 7), there is a significant increase in the values of LI_1 and LI_2 in the first floor (sensors 1–4) indicating damage in the first floor. Similarly, for damage pattern 2 (Table 8),

Table 5
Results of damage decision for damage pattern C (experimental)

Sensor No.	Damage decision	p-value
1	H_1	4.301×10^{-3}
2	H_1	1.583×10^{-2}
3	H_1	5.502×10^{-4}
4	H_1	1.973×10^{-4}
5	H_1	1.836×10^{-4}
6	H_1	8.288×10^{-6}
7	H_1	2.700×10^{-4}
8	H_1	1.120×10^{-6}
9	H_1	9.221×10^{-3}
10	H_1	1.003×10^{-2}
11	H_0	5.277×10^{-2}
12	H_1	2.119×10^{-3}
13	H_1	4.823×10^{-3}
14	H_1	1.129×10^{-3}
15	H_1	1.529×10^{-2}

Table 6
Results of damage decision for damage pattern D (experimental)

Sensor No.	Damage decision	p-value
1	H_1	6.772×10^{-3}
2	H_1	7.958×10^{-3}
3	H_0	5.388×10^{-2}
4	H_1	2.818×10^{-5}
5	H_1	2.174×10^{-5}
6	H_1	1.682×10^{-6}
7	H_1	2.700×10^{-4}
8	H_1	2.899×10^{-3}
9	H_1	5.574×10^{-3}
10	H_1	1.003×10^{-2}
11	H_0	4.053×10^{-6}
12	H_1	3.801×10^{-4}
13	H_1	5.839×10^{-3}
14	H_1	5.853×10^{-3}
15	H_1	7.756×10^{-3}

there is a significant increase in the values of LI_1 and LI_2 for the first and third floors. In the case of damage pattern 3 (Table 9), index LI_1 has a comparatively large value at sensor location 2 in comparison to other sensor locations, indicating damage close to sensor 2. However, the index LI_2 has large values at sensor locations 2 and 4. In the case of damage pattern 4 (Table 10), index LI_1

Table 7
Results of damage localization for damage pattern 1 (simulated)

Sensor No.	LI_1	LI_2
1	2.4951	2.3924
2	1.6787	2.5286
3	2.5094	2.9239
4	1.9262	2.2230
5	0.5721	0.6688
6	0.2155	1.0083
7	0.5655	0.7500
8	0.2476	1.0373
9	0.5494	0.9557
10	0.2405	0.8031
11	0.5167	0.9650
12	0.2573	0.8088
13	0.6094	0.6350
14	0.2768	0.8405
15	0.6040	0.6721
16	0.2312	0.8356

Table 8
Results of damage localization for damage pattern 2 (simulated)

Sensor No.	LI_1	LI_2
1	2.7240	2.8440
2	1.9012	2.0032
3	2.1325	2.4761
4	1.5461	2.2013
5	0.7176	0.9142
6	0.5839	1.3001
7	0.7085	0.9084
8	0.5786	1.2797
9	1.8096	2.6260
10	2.4388	2.8864
11	1.7901	2.3246
12	2.1133	2.8934
13	0.6617	1.5211
14	0.8088	0.9794
15	0.8265	1.6814
16	0.7890	0.9621

has a comparatively large value at sensor locations 2 and 10 in comparison to other sensor locations, indicating damage close to sensors 2 and 10. However, the index LI_2 has large values at sensor locations 2, 4 10 and 12. Thus, LI_1 seems to be a more robust localization index.

Table 9
Results of damage localization for damage pattern 3 (simulated)

Sensor No.	LI_1	LI_2
1	0.8871	0.4142
2	1.2898	2.1296
3	0.8644	0.3424
4	0.8666	1.9382
5	0.6264	0.3764
6	0.6291	1.1750
7	0.2949	0.8994
8	0.5436	1.0802
9	0.7097	0.3758
10	0.5335	0.5275
11	0.5266	0.7640
12	0.5469	0.4941
13	0.4691	0.5214
14	0.4240	1.1373
15	0.4630	1.1725
16	0.6080	0.5380

Table 10
Results of damage localization for damage pattern 4 (simulated)

Sensor No.	LI_1	LI_2
1	0.3710	0.6835
2	1.3446	2.1295
3	0.7575	0.9166
4	0.8911	2.4811
5	0.3490	0.6555
6	0.6241	1.1651
7	0.3519	0.8890
8	0.5531	1.1013
9	0.5342	0.4849
10	1.3642	2.1745
11	0.4391	0.5411
12	0.8312	1.6096
13	0.3519	0.8696
14	0.4245	1.1330
15	0.2267	0.8712
16	0.3304	0.9544

4. Conclusions

In this paper, a damage-detection algorithm based on time series modeling is discussed. A damage sensitive feature, DSF, which is a function of the first three auto regressive (AR) components, is also discussed. A hypothesis test involving the t-test is used to obtain a damage

decision. Two localization indices, LI_1 and LI_2, defined in the AR coefficient space are also introduced. The damage detection and localization methodologies were tested on the analytical and experimental results of the ASCE benchmark structure. The results of the damage detection indicate that the algorithm is able to detect the existence of all damage patterns in the ASCE Benchmark simulation experiment where minor, moderate and severe damage corresponds to removal of single brace, removal of all braces in a story and removal of all braces in two stories, respectively. These results are very encouraging, but represent initial testing of the algorithm and further investigations will be needed to test the validity of the damage-detection method.

The results of the damage localization also indicate that the index LI_1 it is able to localize minor damage patterns. The second localization index, LI_2, appears to be non-conclusive when there is minor damage in the structure. For both, the damage detection and the localization indices considerably more testing is needed to investigate various scenarios and conditions that introduce other damage patterns, such as cracking at joints or loosening of bolts. While it may be difficult to simulate such conditions numerically, they can be reproduced in the laboratory. Thus, additional testing will be performed as such data become available. Ultimately, these algorithms will need to be tested with field data. Such data, however, are not currently available.

The advantage of the statistical signal processing approach combined with the pattern classification framework is that it does not require any elaborate finite element modeling. Such an approach is particularly suited for wireless sensor analysis, which is able to process data at the sensor unit location through embedded algorithms. Such data can then be transmitted to a global master for additional damage analysis using system identification methods.

Acknowledgements

The present research study is supported by the National Science Foundation through Grant No. CMS-0121841. We greatly appreciate their continued support. The first author is supported by the John A. Blume Graduate Research Fellowship. The authors would like to acknowledge the ASCE Benchmark Committee for providing the relevant MATLAB codes.

Appendix A. Eigenvalue and eigenvector sensitivity analysis

The eigenvalues and eigenvectors of a N degree of freedom system is obtained by solving the following eigenvalue problem:

$$\mathbf{K}\mathbf{v}_r - \omega_r^2\mathbf{M}\mathbf{v}_r = 0 \text{ for all } r = 1, \cdots, N, \tag{A.1}$$

where $\mathbf{v}_r$ be the rth eigenvector corresponding to the eigenvalue ω_r^2, and $\mathbf{K}$ and $\mathbf{M}$ are the mass and stiffness matrices, respectively. Differentiating Eq. (A.1) with respect to parameter θ_i (say an element of the stiffness matrix), to obtain

$$\frac{\partial \mathbf{K}}{\partial \theta_i}\mathbf{v}_r + \mathbf{K}\frac{\partial \mathbf{v}_r}{\partial \theta_i} = 2\omega_r \frac{\partial \omega_r}{\partial \theta_i}\mathbf{M}\mathbf{v}_r + \omega_r^2\mathbf{M}\frac{\partial \mathbf{v}_r}{\partial \theta_i}. \tag{A.2}$$

Pre-multiplying with the transpose of $\mathbf{v}_s$ and simplifying to obtain

$$2\omega_r \frac{\partial \omega_r}{\partial \theta_i} \mathbf{v}_s^{\mathrm{T}} \mathbf{M} \mathbf{v}_r = \mathbf{v}_s^{\mathrm{T}} \frac{\partial \mathbf{K}}{\partial \theta_i} \mathbf{v}_r + \left(\omega_s^2 - \omega_r^2\right) \mathbf{v}_s^{\mathrm{T}} \mathbf{M} \frac{\partial \mathbf{v}_r}{\partial \theta_i}. \tag{A.3}$$

Using the orthogonality property and $r = s$, we obtain

$$\frac{\partial \omega_r}{\partial \theta_i} = \frac{1}{2\omega_r \left(\mathbf{v}_r^{\mathrm{T}} \mathbf{M} \mathbf{v}_r\right)} \mathbf{v}_r^{\mathrm{T}} \frac{\partial \mathbf{K}}{\partial \theta_i} \mathbf{v}_r. \tag{A.4}$$

It is also shown in Refs. [16,17] that the eigenvector sensitivity is a linear combination of the eigenvectors, i.e.,

$$\frac{\partial \mathbf{v}_r}{\partial \theta_i} = \sum_{j=1}^{N} \kappa_{rj}^i \mathbf{v}_r, \tag{A.5}$$

where κ_{rj}^i can be derived as [17]

$$\begin{aligned} \kappa_{rj}^i &= \frac{\mathbf{v}_j^{\mathrm{T}} \left((\partial \mathbf{K}/\partial \theta_i) - \omega_r^2 (\partial \mathbf{M}/\partial \theta_i)\right) \mathbf{v}_r}{\omega_r^2 - \omega_j^2} \quad \text{for } r \neq j, \\ &= -\frac{1}{2} \mathbf{v}_j^{\mathrm{T}} \frac{\partial \mathbf{M}}{\partial \theta_i} \mathbf{v}_r \quad \text{for } r = j. \end{aligned} \tag{A.6}$$

Since θ_i is one of the coefficients of the stiffness matrix, we obtain

$$\begin{aligned} \kappa_{rj}^i &= \frac{\mathbf{v}_j^{\mathrm{T}} (\partial \mathbf{K}/\partial \theta_i) \mathbf{v}_r}{\omega_r^2 - \omega_j^2} \quad \text{for } r \neq j, \\ &= 0 \quad \text{for } r = j. \end{aligned} \tag{A.7}$$

To obtain the derivative of the rth modal stiffness with respect to θ_i, $\partial k_r/\partial \theta_i$, differentiate the equation $k_r = \omega_r^2 \, m_r$, we obtain

$$\frac{\partial k_r}{\partial \theta_i} = 2\omega_r m_r \frac{\partial \omega_r}{\partial \theta_i} + 2\omega_r^2 \frac{\partial \mathbf{v}_r^{\mathrm{T}}}{\partial \theta_i} \mathbf{M} \mathbf{v}_r. \tag{A.8}$$

Using Eqs. (A.4) and (A.7), Eq. (A.8) can be expressed as

$$\frac{\partial k_r}{\partial \theta_i} = \mathbf{v}_r^{\mathrm{T}} \frac{\partial \mathbf{K}}{\partial \theta_i} \mathbf{v}_r + 2\omega_r^2 \left[\sum_{\substack{j=1 \\ j \neq r}}^{N} \left(\frac{\mathbf{v}_j^{\mathrm{T}} (\partial \mathbf{K}/\partial \theta_i) \mathbf{v}_r}{\omega_r^2 - \omega_j^2} \right) \mathbf{v}_j \right] \frac{\partial \mathbf{v}_r^{\mathrm{T}}}{\partial \theta_i} \mathbf{M} \mathbf{v}_r. \tag{A.9}$$

This can be further simplified by using the orthogonality principle

$$\frac{\partial k_r}{\partial \theta_i} = \mathbf{v}_r^{\mathrm{T}} \frac{\partial \mathbf{K}}{\partial \theta_i} \mathbf{v}_r. \tag{A.10}$$

Since $\mathbf{v}_r$ is normalized, it can also be shown that

$$\left| \frac{\partial k_r}{\partial \theta_i} \right| \leqslant 1. \tag{A.11}$$

References

[1] F.-K. Chang (Ed.), *Proceedings of the First, Second and Third International Workshops on Structural Health Monitoring*, Stanford University, Stanford, CA, CRC Press, New York, 1997, 1999 and 2001.
[2] E.G. Straser, A.S. Kiremidjian, Modular wireless damage monitoring system for structures, Report No. 128, John A. Blume Earthquake Engineering Center, Department of Civil and Environmental Engineering, Stanford University, Stanford, CA, 1998.
[3] J.P. Lynch, A. Sundararajan, K.H. Law, A.S. Kiremidjian, E. Carryer, Embedding damage detection algorithms in a wireless sensing unit for attainment of operational power efficiency, *Smart Materials and Structures* 13 (4) (2004) 800–810.
[4] S.W. Doebling, C.R. Farrar, M.B. Prime, D.W. Shevitz, Damage identification and health monitoring of structural and mechanical systems from changes in their vibration characteristics: a literature review, Los Alamos National Laboratory Report LA-13070-MS, Los Alamos National Laboratory, Los Alamos, NM 87545, 1996.
[5] H. Sohn, C.R. Farrar, H.F. Hunter, K. Worden, Applying the LANL statistical pattern recognition paradigm for structural health monitoring to data from a surface-effect fast patrol boat, Los Alamos National Laboratory Report LA-13761-MS, Los Alamos National Laboratory, Los Alamos, NM 87545, 2001.
[6] Y. Lei, A.S. Kiremidjian, K.K. Nair, J.P. Lynch, K.H. Law, T.W. Kenny, E. Carryer, A. Kottapalli, Statistical damage detection using time series analysis on a structural health monitoring benchmark problem, *Proceedings of Ninth International Conference on Application of Statistics and Probability in Civil Engineering*, *ICASP*, San Francisco, CA, 2003.
[7] T. Rytter, Vibration Based Inspection of Civil Engineering Structure, PhD Dissertation, Department of Building Technology and Structure Engineering, Aalborg University, Denmark, 1993.
[8] The ASCE Benchmark Group Webpage: http://wusceel.cive.wustl.edu/asce.shm/benchmarks.htm
[9] E.A. Johnson, H.F. Lam, L.S. Katafygiotis, J.L. Beck, A benchmark problem for structural health monitoring and damage detection, *Proceedings of 14th Engineering Mechanics Conference*, Austin, TX, USA, 2000.
[10] S.J. Dyke, D. Bernal, J.L. Beck, C. Ventura, An experimental benchmark problem in structural health monitoring, *Proceedings of Third International Workshop on Structural Health Monitoring*, Stanford, 2001.
[11] P.J. Brockwell, R.A. Davis, *Introduction to Time Series and Forecasting*, second ed., Springer, New York, 2002.
[12] J.A. Rice, *Mathematical Statistics and Data Analysis*, second ed., Duxbury Press, 1999.
[13] N.M.M. Maia, J.M.M. Silva (Eds.), *Theoretical and Experimental Modal Analysis*, Research Studies Press, Hertfordshire, UK, 1998.
[14] J.P. Lynch, Linear classification of system poles for structural damage detection using piezoelectric active sensors, *Proceedings of SPIE 11th Annual International Symposium on Smart Structures and Materials*, San Diego, CA, USA, 2004.
[15] A.V. Oppenheim, R.W. Schafer, *Digital Signal Processing*, first ed, Pearson Higher Education, 1986.
[16] R. Fox, M. Kapoor, Rate of change of eigenvalues and eigenvectors, *AIAA Journal* 6 (1968) 2426–2429.
[17] R.B. Nelson, Simplified calculations of eigenvector derivatives for large dynamic systems, *AIAA Journal* 14 (1976) 1201–1205.